catalysts

MDPI

Article

High-Efficient Calcium-Based Adsorbent for Dry Desulfurization

Lixin Sun * and Qitu Zhang *

College of Materials Science and Engineering, Nanjing Tech University, Nanjing 211816, China
* Correspondence: orijust@163.com (L.S.); zhqt@njtech.edu.cn (Q.Z.)

Abstract

Developing high activity calcium-based adsorbent is still one of the difficult problems for calcium-based adsorbents for dry desulfurization. Herein, we develop the surfactant induction coprecipitation strategy to construct high active layered mesoporous calcium hydroxide. It was found that ethanol as a solvent could modify the lamellar morphology of calcium-based adsorbent, that the surfactant (CTAB) plays an important role in regulating the pore structure to obviously improve the desulfurization activity and utilization efficiency, and that its breakthrough sulfur capacity reaches 371.7 mg g^{-1} at 350 °C. The excellent desulfurization performance is attributed to the unique 2D lamellar morphology, high specific surface area, and mesopore structure of calcium hydroxide. Experimental and theoretical results reveal that SO_2 is preferentially adsorbed on the surface of $Ca(OH)_2$, and reacts with $Ca(OH)_2$ to form $CaSO_3$. $CaSO_3$ is then oxidized by O_2 in the presence of SO_2 and CO_2 to form $CaSO_4$, and the presence of CO_2 inhibited the catalytic oxidation of sulfite to sulfate by O_2 from air. This synthesis strategy offers a facile method to construct efficient 2D adsorbent for SO_2 removal.

Keywords: calcium hydroxide; adsorbent; layered nanosheets; surfactant induction synthesis; coprecipitation method

1. Introduction

Sulfur dioxide (SO_2) is one of the main air pollutants, which cause serious pollution and damage to the ecological environment [1]. The coal, iron, and steel industries, as well as other fields, all involve the treatment of SO_2-containing gas [2,3]. At present, desulfurization technology is the main technical means to control SO_2 pollution. Flue gas desulfurization (FGD) technology is the most effective desulfurization technology, which directly contacts the adsorbent to remove SO_2. In this technology, the adsorbent is the key to determine the desulfurization performance of FGD [4]. At present, FGD technology is mainly divided into wet, semi-dry, and dry methods [5,6]. Dry desulfurization is realized by gas–solid reaction. The solid adsorbents contain Ca-based adsorbents [7–10], Na-based adsorbents [11–13], carbon-based adsorbents [14], zeolites [15], composite metal oxides [16], and so on, among which the most commonly used solid adsorbent is a calcium-based adsorbent. During dry adsorption processes, calcium-based adsorbents are widely used in FGD technology because of its widespread availability and low price, and because the corresponding desulfurization products have good high-temperature resistance [17,18].

Calcium hydroxide ($Ca(OH)_2$), as a typical representative of calcium-based adsorbents, is one of the most promising dry adsorbents because of its high activity, suitability for medium-low temperature reaction, no waste water, low water consumption, and easy treatment of products in dry state [19]. However, SO_2 reacts rapidly on the surface of

Academic Editor: Lucjan Chmielarz

Received: 26 March 2026
Revised: 21 April 2026
Accepted: 23 April 2026
Published: 29 April 2026

$Ca(OH)_2$ to generate sulfate, and the sulfate product wraps the surface of $Ca(OH)_2$, blocking its further desulfurization reaction, which leads to the decrease of desulfurization efficiency and the relatively low desulfurization activity of calcium-based adsorbents. Therefore, it has become one of the challenges for dry desulfurization of industrial flue gas to improve the utilization efficiency of $Ca(OH)_2$. In recent years, many efforts have been made to modify $Ca(OH)_2$, including its size [20], morphology [21], pore structure [22], metal doping [23], and composite process [24] of the adsorbents, which increased the specific surface area of the calcium-based adsorbents and improved the exposure of active sites, thus enhancing the desulfurization activity of the adsorbents. For example, Rendo et al. [25] reported the organic lignosulfonate (LGSs) modified $Ca(OH)_2$ adsorbent, and found that LGSs could effectively improve the porosity of calcium-based adsorbent. Ishizuka et al. [26] prepared calcium-based adsorbent by hydrothermal method using CaO and fly ash as precursors, and found that SiO_2 component in fly ash could be converted into activated calcium silicate during hydrothermal process, thus improving the surface structure of calcium-based adsorbent and greatly improving its desulfurization efficiency; The ethanol solution could also hydrate calcium oxide to increase the specific surface area and desulfurization efficiency of calcium-based adsorbent [19]. In addition, the introduction of metal elements such as Ce, Fe, Co, Mn, etc. is helpful to promote SO_2 oxidation, and also improves the desulfurization performance of calcium-based adsorbents [23,24,27]. Therefore, it is desirable to construct novel calcium-based adsorbent with high desulfurization efficiency and utilization efficiency. In addition, the presence of CO_2 in actual flue gas also adversely affects the desulfurization efficiency of adsorbents [28]. The adsorption competition of CO_2 and SO_2 on the surface of adsorbents results in the reduction of effective adsorption sites of SO_2 and the decrease of adsorption capacity [9,29], and the mechanism of inhibiting desulfurization remains to be further explored.

In this study, we constructed layered mesoporous $Ca(OH)_2$ via a facile surfactant-induced coprecipitation method for high efficient SO_2 removal in dry desulfurization. By optimizing synthesis conditions such as the solvent and surfactant, the as-prepared adsorbent demonstrated excellent desulfurization efficiency, achieving a breakthrough sulfur capacity of 371.7 mg g^{-1} with high utilization efficiency of the adsorbent. The as-prepared $Ca(OH)_2$ adsorbents were investigated using comprehensive characterizations to identify the physical and chemical properties, including morphological features (SEM, TEM), chemical valence states (XPS), and pore structure (BET), to investigate the relationship between the adsorbent's properties and their desulfurization performance. Moreover, in situ DRIFTS investigations provided mechanistic insights into intermediate species formation during SO_2 removal process on active sites of adsorbent.

2. Results

2.1. Synthesis of Ca-Based Adsorbents

Mesoporous lamellar $Ca(OH)_2$ was synthesized via a facile coprecipitation method using ethanol as solvent, as illustrated in Scheme 1. $CaCl_2$ was chosen as a calcium precursor and CTAB micelle as a pore former. The calcium precursor and CTAB were dissolved in the ethanol solvent. Then, the NaOH ethanol solution was added dropwise to the above solution. The precursor was then further washed with ethanol to obtain mesoporous $Ca(OH)_2$ nanosheets. Figure 1a,b showed that CaOH-W exhibited a bulk rod structure with a size of 1–5 μm. In order to investigate the growth mechanism of lamellar $Ca(OH)_2$, ethanol was added to a water solution, as shown in Figure S1. Figure S1c,d showed that when ethanol was added to the aqueous solution, the size of the $Ca(OH)_2$ obviously changed, and the particle size was in the range of 0.5–1 μm, indicating that the existence of ethanol was more conducive to the nucleation of $Ca(OH)_2$. Ethanol molecules

might be used as "capping agents" and selectively adsorbed on specific crystal faces of $Ca(OH)_2$ crystals. Further increasing the proportion of ethanol, the morphology of $Ca(OH)_2$ gradually transformed into the lamellar structure, and its size remained in the range of 0.5–1 μm (Figure S1e–j). When ethanol was used as the solvent instead of water, CaOH-E exhibited a layered structure (as shown Figure 1c,d), where the size of the particles was in the range of 0.50–1.0 μm, suggesting that ethanol was beneficial to induce calcium ions and hydroxyl ions to form a nanosheet structure during the co-precipitation process. However, when cetyltrimethyl ammonium bromide (CTAB) was added to the ethanol solution, Figure 1e,f showed that the CaOH-E-C sample still maintained its lamellar morphology. This result indicated that the introduction of the surfactant did not affect the morphology and particle size of calcium hydroxide.

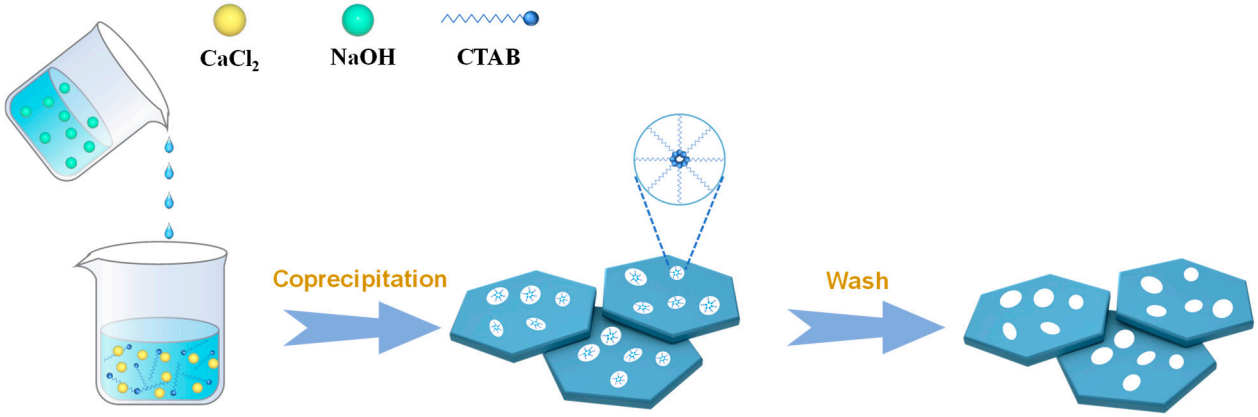

Scheme 1. Illustration for the preparation of lamellar $Ca(OH)_2$.

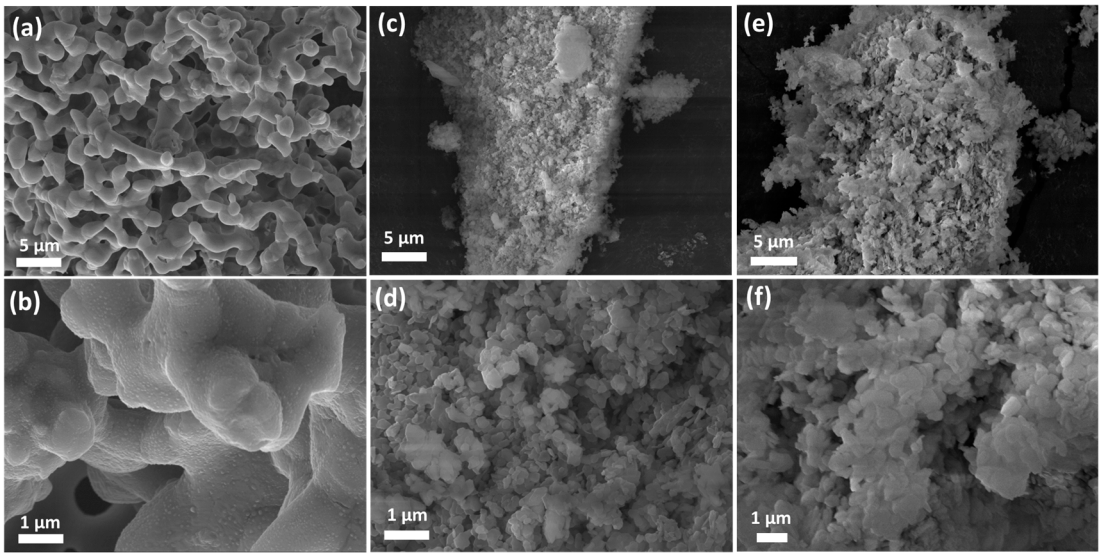

Figure 1. SEM images (**a**,**b**) CaOH-W, (**c**,**d**) CaOH-E, (**e**,**f**) CaOH-E-C.

2.2. Morphology and Structure of Ca-Based Adsorbents

Figure 2a–d showed that CaOH-E-C exhibited a layered structure, and the crystal plane spacing (d) of CaOH-E-C was 0.18 nm and 0.27 nm, respectively, corresponding to the (110) and (101) crystal planes of hexagonal calcium hydroxide. As adsorbents for dry desulfurization, Figure 3a,b showed that CaOH-W had low desulfurization activity with a breakthrough sulfur capacity of 72.7 mg g^{-1}, and CaOH-E exhibited obviously enhanced desulfurization activity with a breakthrough sulfur capacity of 136.6 mg g^{-1}. This result indicated that the 2-dimensional structure could expose more active sites for adsorption of

SO_2. Surprisingly, CaOH-E-C had the highest desulfurization activity, with a breakthrough sulfur capacity of 371.7 mg g^{-1}, suggesting that the CTAB played an important role in enhancing the desulfurization activity. Figure S2 showed that the desulfurization activity of CaOH-E-C increased as the temperature was rose from 300 °C to 350 °C. Upon increasing the temperature to 400 °C, the desulfurization activity decreased, with the optimal temperature being 350 °C. The XRD spectra of the as-prepared calcium-based adsorbents were shown in Figure 3c. All adsorbents had the characteristic diffraction peaks of hexagonal $Ca(OH)_2$ (standard PDF card: 44-1481), suggesting that $Ca(OH)_2$ adsorbents were successfully synthesized by the coprecipitation method with different solvents.

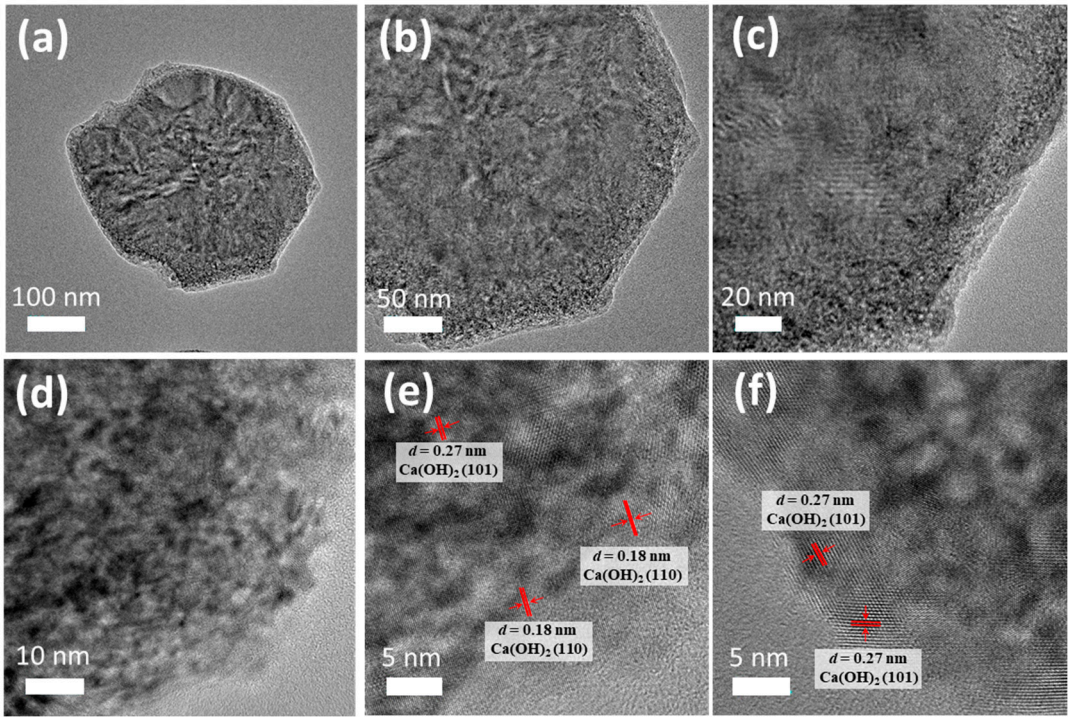

Figure 2. (**a**–**f**) TEM images of CaOH-E-C.

2.3. Structure–Activity Relationship of Ca-Based Adsorbents

The porosity structure of the samples was studied via N_2 adsorption–desorption isotherms (Figure 3d). It was found that CaOH-E-C exhibited a type IV isotherm with a characteristic H3 hysteresis loop, attributable to plate-like materials, and wide pore size distributions (20–80 nm) were observed (Figure 3e), which could be attributed to slit-like pores formed between $Ca(OH)_2$ nanosheets. CaOH-E-C had a higher specific surface area of 20 m^2 g^{-1} and a larger pore volume of 0.17 cm^3 g^{-1} compared to those of CaOH-W (8 m^2 g^{-1}, 0.07 cm^3 g^{-1}) and CaOH-E (10 m^2 g^{-1}, 0.14 cm^3 g^{-1}), indicating the superiority of our micellar template induction strategy to construct a mesoporous structure within the nanosheets during the coprecipitation process. Figure 3f showed the simultaneous TG-DSC curves of CaOH-E-C. It was found that there was an obvious weight loss of 21.2% from 350 °C to 550 °C, accompanied by an endothermic peak at 421 °C, which could be attributed to the decomposition of most of the calcium hydroxide. This might be the reason why the desulfurization activity of the adsorbent decreased due to excessive temperature (>350 °C). The weight loss of 4.9% from 550 to 660 °C, accompanied bt an endothermic peak around 626 °C, could be attributed to the decomposition of residual calcium hydroxide. Over 660 °C, the weight loss of CaOH-E-C could hardly be observed, indicating that the calcium hydroxide had been completely decomposed.

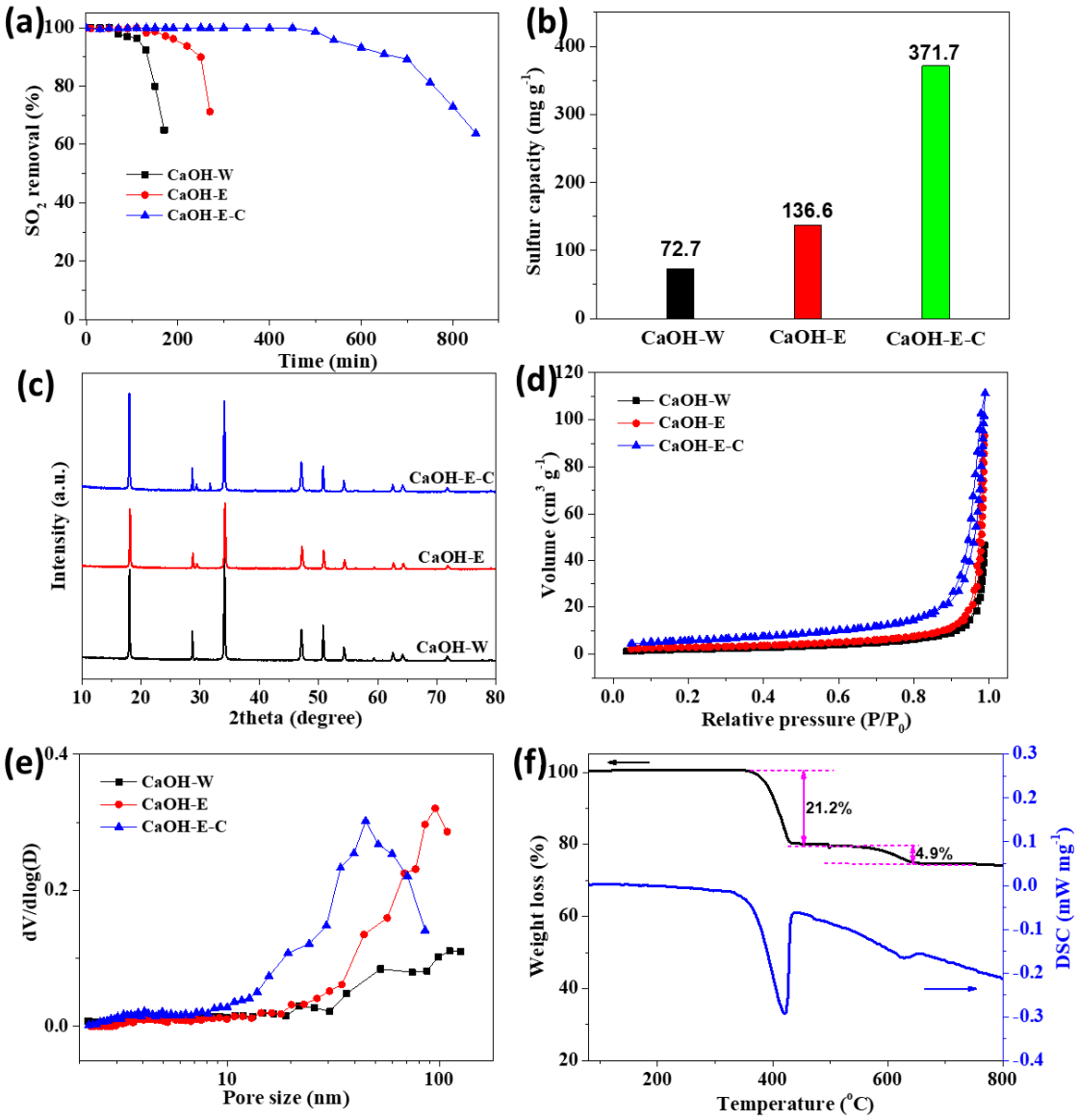

Figure 3. (**a**) Desulfurization curves and (**b**) the corresponding breakthrough sulfur capacity of CaOH-W, CaOH-E, and CaOH-E-C in fixed-bed adsorbents. (**c**) XRD patterns, (**d**) N_2 sorption curves, and (**e**) the corresponding pore size distribution of CaOH-W, CaOH-E, and CaOH-E-C. (**f**) TG-DSC curve of CaOH-E-C.

After desulfurization, the XRD patterns of the desulfurized adsorbents were shown in Figure 4a. CaOH-W still exhibited the characteristic diffraction peak of hexagonal $Ca(OH)_2$ (standard PDF card: 44-1481), suggesting that $Ca(OH)_2$ adsorbents had low utilization efficiency. For CaOH-E, in addition to the diffraction peaks of $Ca(OH)_2$, the diffraction peak of $CaSO_4$ and $CaSO_3$ also appeared, demonstrating the higher desulfurization activity of CaOH-E compared to CaOH-W. Notably, only the characteristic diffraction peaks of $CaSO_4$ and $CaSO_3$ were observed, and the diffraction peak of hexagonal $Ca(OH)_2$ disappeared. This result further revealed the higher desulfurization activity and superior utilization efficiency of CaOH-E-C. The surface element chemical states of the desulfurized adsorbents were analyzed by X-ray photoelectron spectroscopy (XPS). Figure 4b showed the high-resolution S 2p XPS spectra of the desulfurized adsorbents. The S $2p_{3/2}$ peaks of three desulfurized adsorbents were fitted into two peaks at 168.83 eV and 166.87 eV, assigned to SO_4^{2-} and SO_3^{2-}, respectively [30]. This result indicated that SO_2 reacted with calcium hydroxide to form calcium sulfate and calcium sulfite on the surface of CaOH-E-C.

The calcium sulfite and calcium sulfate formed in CaOH-E-C accounted for the highest proportion, which was consistent with the results of XRD (Figure 4a). This result suggested that surfactants might play a catalytic role in promoting desulfurization activity.

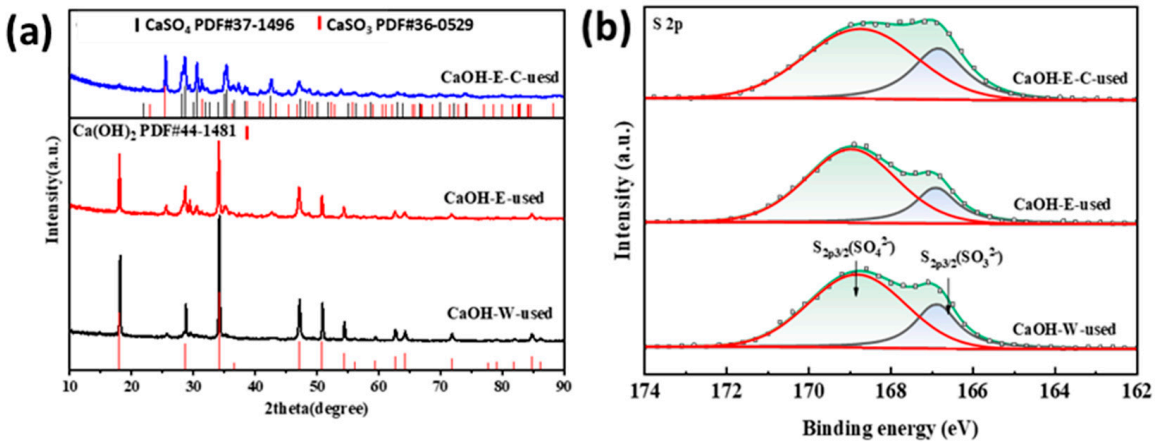

Figure 4. (**a**) XRD patterns, (**b**) High-resolution S 2p spectra of CaOH-W, CaOH-E and CaOH-E-C adsorbents after desulfurization.

2.4. Desulfurization Mechanism of Ca-Based Adsorbents

The actual flue gas contains a certain amount of CO_2, which had a certain influence on the adsorbent for dry desulfurization. Figure 5a,b showed that the desulfurization activity of the CaOH-E-C adsorbent was significantly reduced, with a breakthrough sulfur capacity of 181.5 mg g^{-1} in the presence of CO_2, indicating that CO_2 had an inhibitory effect on desulfurization. In addition, Figure S3 showed that the presence of H_2O and NO had little effect on the desulfurization activity for CaOH-E-C.

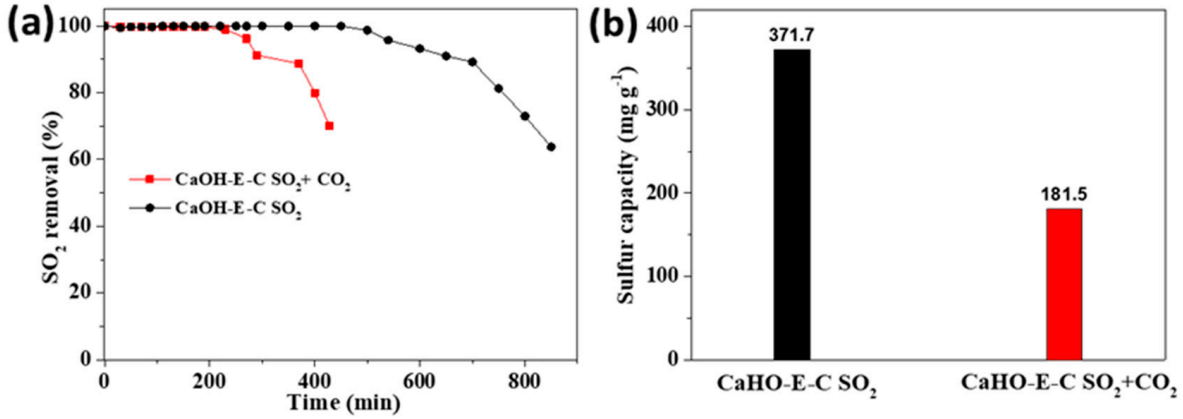

Figure 5. (**a**) Desulfurization curves and (**b**) the corresponding breakthrough sulfur capacity of CaOH-E-C in fixed-bed adsorbents with SO_2 and SO_2 + CO_2 conditions.

In order to further study the effect of CO_2 on the desulfurization performance of the CaOH-E-C adsorbent, in situ DRIFTS analysis of CaOH-E-C was carried out under various gas conditions (Figure 6). Figure 6a showed in situ DRIFTS spectra at 200 °C followed by the adsorption of SO_2 on the surface of CaOH-E-C. Three bands were observed at 1355 cm^{-1}, 1140 cm^{-1}, and 940 cm^{-1}. The bands at 1355 cm^{-1} and 940 cm^{-1} belonged to the characteristic peaks of sulfite (SO_3^{2-}), and the band at 1140 was assigned to the characteristic peak of sulfate (SO_4^{2-}) [31,32]. This result indicated that SO_2 generated $CaSO_4$ and $CaSO_3$ on the surface of CaOH-E-C, the peak at 1140 cm^{-1} gradually increased with time, the desulfurization reaction gradually progressed, and the peak intensity of

calcium sulfate gradually increased. The results indicated that SO_2 was adsorbed on the surface of CaOH-E-C and underwent a desulfurization reaction to form sulfite, which was then oxidized to sulfate by oxygen in the air. After 30 min of desulfurization, SO_2 was stopped and CO_2 gas was introduced instead. As illustrated in Figure 6b, with the extension of the CO_2 introduction time, a small peak gradually appeared near 2307 cm^{-1}, which belonged to the band of adsorbed CO_2. With the extension of time, the intensity of this band did not change, indicating that CO_2 was adsorbed on the surface of CaOH-E-C and reached adsorption saturation.

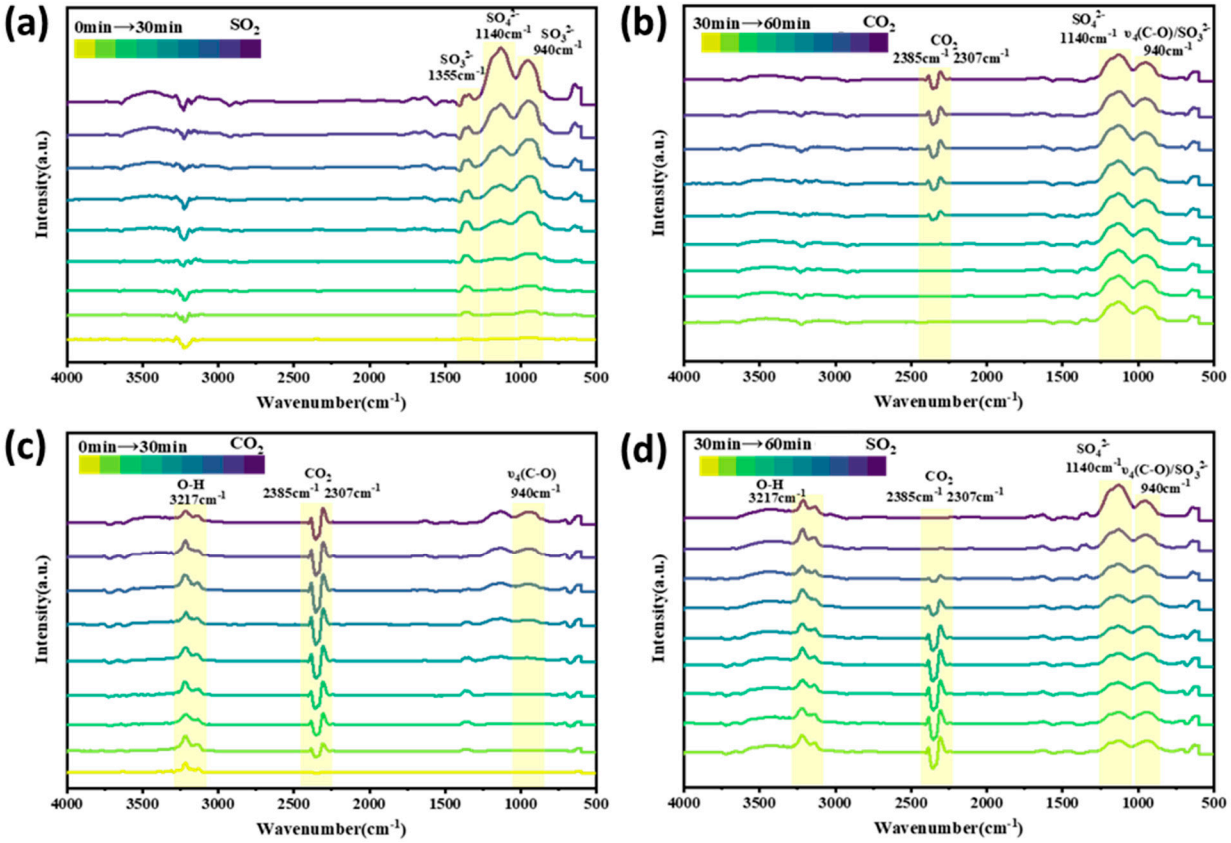

Figure 6. In situ DRIFTS spectra of CaOH-E-C under (**a**) SO_2 gas condition at 200 °C, (**b**) then CO_2 gas condition over preadsorbed SO_2 at 200 °C, (**c**) CO_2 gas condition at 200 °C, (**d**) SO_2 gas condition over preadsorbed CO_2 at 200 °C.

Figure 6c displayed in situ DRIFTS spectra at 200 °C followed by the adsorption of CO_2 on the surface of CaOH-E-C. When CO_2 gas was introduced, the band near 940 cm^{-1} appeared slowly. This band belonged to the characteristic peak of carbonate (CO_3^{2-}), indicating that CO_2 reacted with hydroxyl on the surface of CaOH-E-C to generate calcium carbonate, and the intensity of this characteristic peak slowly increased with time [33]. At the same time, a band gradually appeared near 2307 cm^{-1}, which belonged to the band of adsorbed CO_2. With the extension of time, the intensity of this band no longer changed, indicating that CO_2 reached adsorption saturation on the surface of CaOH-E-C. After 30 min, CO_2 was stopped and SO_2 was introduced instead. As shown in Figure 6d, two new bands appeared near 1140 cm^{-1} and 1355 cm^{-1} as time extended, indicating that SO_2 reacted with hydroxyl on the surface of CaOH-E-C to generate sulfate and sulfite. With the prolongation of the SO_2 introduction time, the characteristic peak of CO_2 adsorbed on the surface of CaOH-E-C and gradually weakened until it disappeared. The acidity of SO_2 was stronger than that of CO_2; therefore, SO_2 gradually replaced CO_2, which led to the band of CO_2 gradually weakening until it disappeared.

In situ DRIFTS spectra of CaOH-E-C, followed by the adsorption of SO_2 and CO_2 at 200 °C, were shown in Figure 7. After CO_2 and SO_2 were simultaneously introduced, a new band gradually appeared near 2307 cm^{-1}, which belonged to the band of adsorbed CO_2. The intensity of this band did not change with time, indicating that the CO_2 had reached adsorption saturation on the surface of CaOH-E-C. The adsorption of CO_2 occupied parts of the alkaline sites of CaOH-E-C, thus reducing the desulfurization performance of CAOH-E-C. With the extension of time, characteristic absorption peaks appeared around 1355 cm^{-1}, 1140 cm^{-1}, and 940 cm^{-1}, and the band at 940 cm^{-1}, which belonged to the characteristic band of both sulfite and carbonate, indicated that SO_2 and CO_2 underwent a desulfurization reaction on the surface of CaOH-E-C to generate calcium sulfate (related to 1140 cm^{-1}), calcium sulfite (related to 1355 cm^{-1} and 940 cm^{-1}), and calcium carbonate (related to 940 cm^{-1}). It is worth noting that the peak intensity of sulfite was much higher than that of sulfate, indicating that, in the presence of CO_2, the desulfurization product was mainly calcium sulfite, and CO_2 inhibited the catalytic oxidation of sulfite to sulfate by O_2 from air.

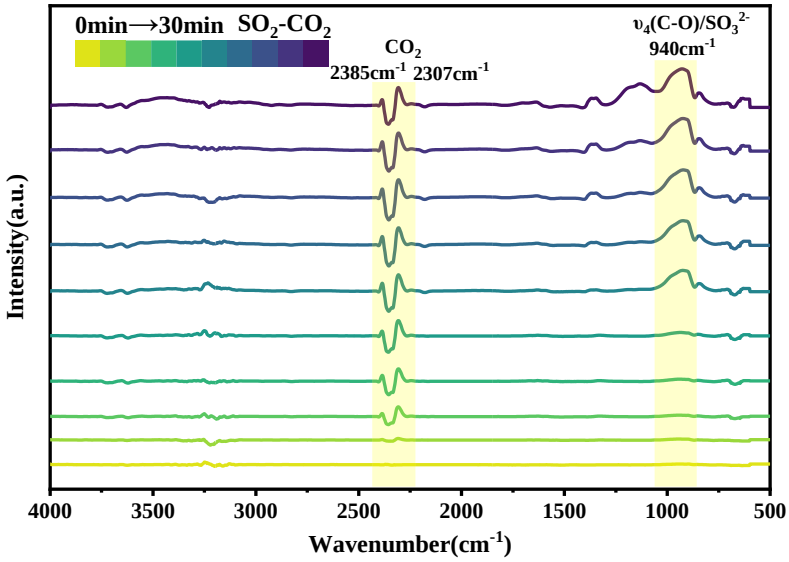

Figure 7. In situ DRIFTS spectra of CaOH-E-C under CO_2 + SO_2 gas conditions at 200 °C.

There were four adsorption sites on the (101) crystal plane model of $Ca(OH)_2$ in CaOH-E-C adsorbent as shown in Figure 8. SO_2 was introduced into the surface of $Ca(OH)_2$ to adsorb two SO_2 molecules, and the average adsorption energy of two SO_2 molecules was −0.83 eV. Then, CO_2 was introduced to adsorb two other CO_2 molecules, and the average adsorption energy of the two CO_2 molecules was −0.36 eV. It can be seen that the adsorption capacity of the adsorbent for SO_2 was much higher than that for CO_2. However, when CO_2 was introduced into the surface of $Ca(OH)_2$, two CO_2 molecules were adsorbed onto the (101) crystal plane, and the average adsorption energy of the two CO_2 molecules was −0.40 eV, which was lower than that of SO_2 (−0.83 eV), suggesting that SO_2 was more easily adsorbed on calcium hydroxide than CO_2. Then, SO_2 gas was introduced, two SO_2 molecules were adsorbed onto the other two adsorption sites, and the average adsorption energy of the two SO_2 molecules was −3.00 V. The results demonstrated that whether CO_2 existed or not, the adsorption energy of SO_2 on the surface of calcium hydroxide was higher than that of CO_2. Compared with CO_2, SO_2 was more easily adsorbed on the surface of the adsorbent and reacted with it, while CO_2 and SO_2 compete for adsorption, which reduced the desulfurization activity of the CaOH-E-C adsorbent. This was consistent with the results in Figure 7.

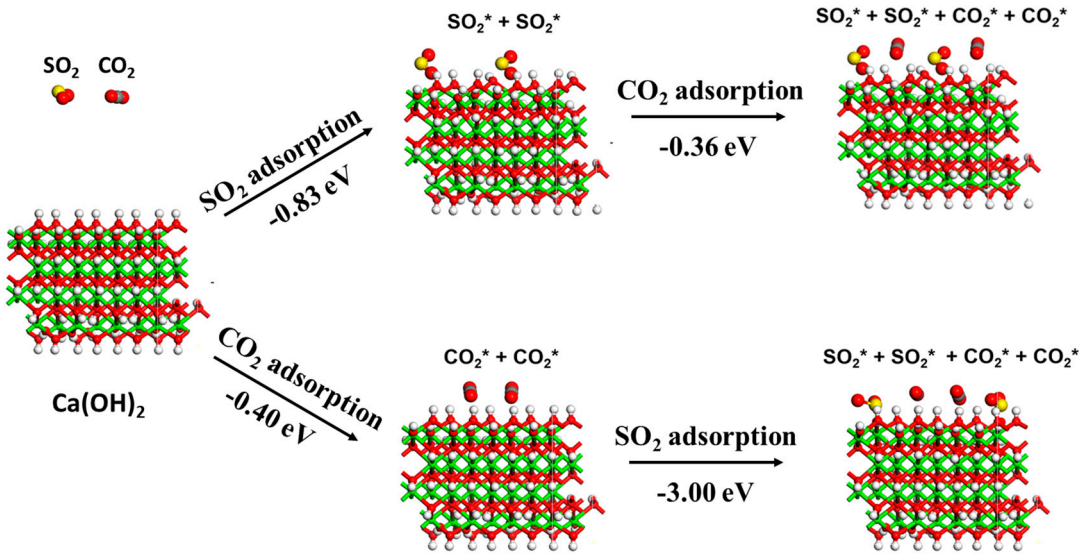

Figure 8. Changes of adsorption energy of CaOH-E-C adsorbent before and after adsorption of SO_2 and CO_2 (*: adsorption state).

3. Materials and Methods

3.1. Synthesis of Calcium-Based Adsorbent

A series of calcium-based adsorbents were synthesized via a coprecipitation method. Firstly, 100 mmol of $CaCl_2$ was dissolved in 60 mL of ethanol to form solution A, and 200 mmol of NaOH and an amount of CTAB was dissolved in 60 mL of ethanol to form solution B. Then, solution B was added into solution A and vigorously stirred for 1 h. Finally, the above mixture solution was centrifuged, washed with ethanol, and dried at 120 °C for 12 h to obtain the $Ca(OH)_2$ sample (denoted as CaOH-E-C).

For comparison, we prepared a calcium-based adsorbent using a similar synthesis process without adding the CTAB, corresponding to the $Ca(OH)_2$ sample (denoted as CaOH-E). The $Ca(OH)_2$ sample (denoted as CaOH-W) also was synthesized using a similar synthesis process using deionized water as solvent. Firstly, 100 mmol of $CaCl_2$ was dissolved in 60 mL of deionized water to form solution A, and 200 mmol of NaOH was dissolved in 60 mL of deionized water to form solution B. Then, solution B was added into solution A and vigorously stirred for 1 h. Finally, the above mixture solution was centrifuged, washed with deionized water, and dried at 120 °C for 12 h to obtain the $Ca(OH)_2$ sample (denoted as CaOH-W).

3.2. Characterization

The crystal structure of the adsorbent was investigated by X-ray diffraction (Smart Lab-9, Rigaku, Tokyo, Japan) using Cu Kα radiation (λ = 0.154 nm) in the scanning range (2θ) of 10–80°. The N_2 adsorption and desorption isotherms of the adsorbent were recorded via N_2 sorption analyzer (iPore400, PhysiChem Instruments Ltd., Beijing, China) at 77 K. Morphological features were examined by field-emission SEM (JSM-7800F, JEOL, Tokyo, Japan) and high-resolution TEM (JEM-F200, JEOL, Tokyo, Japan). Surface acid behavior was probed via CO_2-TPD (AutoChem II 2920, Micromeritics, Norcross, GA, USA). Surface element chemical states were investigated using XPS (Thermo Scientific, Waltham, MA, USA). Thermogravimetric analysis was performed on a thermogravimetric analyzer (HCT-1, Beijing Hengjiu, Beijing, China). In situ DRIFTS (Bruker, Billerica, MA, USA) spectra were acquired under flowing reactants, including SO_2 and CO_2.

3.3. Desulfurization Performance

The desulfurization performance of the prepared calcium hydroxide adsorbent was evaluated using a fixed bed device. The desulfurization device is shown in Figure 1. A total of 0.6 mL of calcium hydroxide adsorbent (mesh number: 40–60 mesh) was placed in a quartz reactor (D = 10 mm), with SO_2 concentration of (400 ppm), O_2 concentration of 4%, N_2 as balance gas, and simulated flue gas space velocity (GHSV) of 20,000 h^{-1}. The desulfurization efficiency (SO_2 removal, %) and penetrating sulfur capacity (S, mg g^{-1}) were used to evaluate the desulfurization performance of the adsorbent. The concentrations of SO_2 at the inlet (φ_0) and outlet (φ_i) of the reactor were measured online by the flue gas analyzer. Its calculation formula is:

$$SO_2 \text{ removal} = (\varphi_0 - \varphi_i)/\varphi_0 \times 100\% \quad (1)$$

The desulfurization efficiency of 90% is commonly taken as the critical efficiency to evaluate the performance of the adsorbent. In this study, breakthrough sulfur capacity is an important index to measure the desulfurization ability, indicating that the quality of SO_2 absorbed by each gram of adsorbent before the desulfurization efficiency is 90%. When SO_2 content of >40 ppm was detected for the first time at the outlet of the fixed bed, it is determined as the breakthrough point. The breakthrough sulfur capacity (denoted as Sulfur capacity) is calculated by Equation (2).

$$S = [\sum(\varphi_0 - \varphi_i) \times t_i] \times V/m \quad (2)$$

where t_i is the data recording interval (min), V is the total simulated flue gas flow (mL/min), and m is the mass of adsorbent (g).

3.4. Model Construction and Computational Method

The model of bulk $Ca(OH)_2$ was built according to previous experimental literature [34]. The space group of bulk $Ca(OH)_2$ is P−3m1, with lattice parameters of a = b = c = 3.59 Å, $\alpha = \beta = 90°$, and $\gamma = 120°$. Then, the (101) surface of $Ca(OH)_2$ was cleaved, containing four layers of atoms and a vacuum layer of 20 Å. All calculations in this work were performed with the Cambridge sequential total energy package version 20.1.1 [35]. The spin-polarized density functional theory calculations were performed using a plane wave implementation. The exchange–correlation functional is a Perdew–Burke–Ernzerhof (PBE) generalized gradient approximation (GGA) [36]. The DFT-D correction was performed using the Tkatchenko–Scheffler method. The cutoff energy was set as 500 eV. During geometry optimization, energy tolerance of 5×10^{-5} eV per atom, displacement tolerance of 5×10^{-3} Å, and force tolerance of 0.1 eV $Å^{-1}$ were employed. The k-point meshes were set as gamma k-point.

4. Conclusions

In summary, high active mesoporous lamellar $Ca(OH)_2$ was constructed by the surfactant induction coprecipitation method for dry desulfurization. The as-prepared CaOH-E-C adsorbent exhibited highly efficient desulfurization activity with a breakthrough sulfur capacity of 371.7 mg g^{-1} at 350 °C. The surfactant CTAB played an important role in enhancing the specific surface area and pore volume of $Ca(OH)_2$, and in boosting the desulfurization activity and utilization efficiency of $Ca(OH)_2$. The experimental and theoretical results displayed that SO_2 preferentially reacts with $Ca(OH)_2$ in the presence of SO_2 and CO_2 to form calcium sulfite, and the presence of CO_2 could inhibit the formation of $CaSO_4$ from $CaSO_3$ by oxidation of O_2. This surfactant induction strategy provided a facile method to develop efficient adsorbent for dry desulfurization.

Supplementary Materials: The following supporting information can be downloaded at: https://www.mdpi.com/article/10.3390/catal16050391/s1. Figure S1: SEM images (a,b) CaOH-W, (c,d) CaOH-1E/2W, (e,f) CaOH-1E/1W, (g,h) CaOH-2E/1W, and (i,j) CaOH-E; Figure S2: Desulfurization curves of CaOH-E-C at different temperatures in a fixed bed; Figure S3: Desulfurization curves of CaOH-E-C in a fixed bed adsorbents with SO_2 and SO_2 + NO + H_2O conditions.

Author Contributions: L.S.: Writing—review & editing, Writing—original draft, Supervision, Resources, Investigation, Formal analysis, Conceptualization; Q.Z.: Writing—review& editing, Writing—original draft, Visualization, Resources, Funding acquisition. All authors have read and agreed to the published version of the manuscript.

Funding: This research was funded by Science and Technology Cooperation Project of Fujian Province, grant number 2025T3033.

Data Availability Statement: The original contributions presented in this study are included in the article and Supplementary Materials.

Conflicts of Interest: The authors declare no conflicts of interest.

References

1. Han, R.; Sun, F.; Gao, J.; Wei, S.; Su, Y.; Qin, Y. Trace Na_2CO_3 Addition to Limestone Inducing High-Capacity SO_2 Capture. *Environ. Sci. Technol.* **2017**, *51*, 12692–12698. [CrossRef]
2. Zhang, Z.; Tang, M.; Yang, Z.; Ma, J.; Liu, L.; Shen, B. SO_2 and NO emissions during combustion of high-alkali coal over a wide temperature range: Effect of Na species and contents. *Fuel* **2022**, *309*, 122212. [CrossRef]
3. Cui, L.; Liu, M.; Yuan, X.; Wang, Q.; Ma, Q.; Wang, P.; Hong, J.; Liu, H. Environmental and economic impact assessment of three sintering flue gas treatment technologies in the iron and steel industry. *J. Clean. Prod.* **2021**, *311*, 127703. [CrossRef]
4. Li, X.; Han, J.; Liu, Y.; Dou, Z.; Zhang, T.-A. Summary of research progress on industrial flue gas desulfurization technology. *Sep. Purif. Technol.* **2022**, *281*, 119849. [CrossRef]
5. Kumar, L.; Jana, S.K. Advances in absorbents and techniques used in wet and dry FGD: A critical review. *Rev. Chem. Eng.* **2022**, *38*, 843–880. [CrossRef]
6. Xie, D.; Wang, H.; Chang, D.; You, C. Semidry Desulfurization Process with In Situ Supported Sorbent Preparation. *Energy Fuels* **2017**, *31*, 4211–4218. [CrossRef]
7. Lin, R.-B.; Shih, S.-M. Characterization of $Ca(OH)_2$/fly ash sorbents for flue gas desulfurization. *Powder Technol.* **2003**, *131*, 212–222. [CrossRef]
8. Karatepe, N.; Erdoğan, N.; Ersoy-Meriçboyu, A.; Küçükbayrak, S. Preparation of diatomite/$Ca(OH)_2$ sorbents and modelling their sulphation reaction. *Chem. Eng. Sci.* **2004**, *59*, 3883–3889. [CrossRef]
9. Li, Y.; Buchi, S.; Grace, J.R.; Lim, C.J. SO_2 Removal and CO_2 Capture by Limestone Resulting from Calcination/Sulfation/Carbonation Cycles. *Energy Fuels* **2005**, *19*, 1927–1934. [CrossRef]
10. Bai, Y.J.; Chen, M.Q.; Li, Q.H.; Huang, Y.W. Sulfation performance of CaO under circulating fluidized bed combustion-like condition. *J. Therm. Anal. Calorim.* **2020**, *142*, 1031–1042. [CrossRef]
11. Wang, H.; Lin, L.; Zhao, Z.; Huang, S.; Lū, J.; Li, H.; Liu, Z.; Chen, H. Trace-amount phenolphthalein surface-modified Na_2CO_3 for enhanced low-temperature dry SO_2 capture via altered product layer structure. *J. Hazard. Mater.* **2026**, *501*, 140823. [CrossRef]
12. Lū, J.; Fu, Y.; Wang, J.; Chen, H. Study on the desulfurization performance of calcium-based desulfurizer and $NaHCO_3$ desulfurizer. *Environ. Sci. Pollut. Res.* **2023**, *30*, 20357–20368. [CrossRef]
13. Wang, H.; Lin, L.; Lū, J.; Huang, S.; Li, H.; Chen, H.; Zhao, Z. A novel method for gas-solid contact visualization and efficiency quantification in dry fixed-bed desulfurization. *Sep. Purif. Technol.* **2025**, *355*, 129463. [CrossRef]
14. Zhang, M.; Liang, C.; Duan, L.; Chen, H. Fe-Ce modified biochar reinforced CaO-Char system enables efficient simultaneous SO_2/CO_2 removal: By enhancing synergistic SO_2 reduction in the carbonation step. *Chem. Eng. J.* **2025**, *525*, 170851. [CrossRef]
15. Zhang, Z.; Liu, Y.; Hu, Y.; Gu, S.; Wang, J.; Shen, Y.; Li, P. Facile fabrication of efficient Cu(I)–Y zeolite adsorbent towards the adsorption desulfurization. *Micropor. Mesopor. Mater.* **2023**, *350*, 112450. [CrossRef]
16. Salvitti, C.; Rosi, M.; Pepi, F.; Troiani, A.; de Petris, G. Reactivity of transition metal dioxide anions MO^{2-} (M = Co, Ni, Cu, Zn) with sulfur dioxide in the gas phase: An experimental and theoretical study. *Chem. Phys. Lett.* **2021**, *776*, 138555. [CrossRef]
17. Wang, C.; Shen, X.; Xu, Y. Investigation on sulfation of modified Ca-based sorbent. *Fuel Process. Technol.* **2002**, *79*, 121–133. [CrossRef]
18. Juan, L.; Yu, F.; Lihua, H.; Deliang, T.; Haiyan, C.; Belzile, N.; Yuwei, C. Preparation of a new high-performance calcium-based desulfurizer using a steam jet mill. *J. Hazard. Mater.* **2020**, *389*, 121914. [CrossRef]

19. Xing, G.; Li, S.; Wang, Y.; Zhang, Y.; Wang, W.; Qi, L. Experimental study on the preparation of desulfurizer for low temperature dry desulfurization by digesting CaO in urea solution. *J. Environ. Chem. Eng.* **2024**, *12*, 113865. [CrossRef]
20. Shin, H.-G.; Kim, H.; Kim, Y.-N.; Lee, H.-S. Preparation and characterization of high surface area calcium hydroxide sorbent for SO2 removal. *Curr. Appl. Phys.* **2009**, *9*, S276–S279. [CrossRef]
21. Ma, X.; Wu, H.; Chang, L.; Wang, J.; Wang, Y.; Cui, S. The influence of calcium hydroxide crystal morphology on the desulfurization of cement kiln flue gas. *J. Mater. Sci.* **2022**, *57*, 18287–18297. [CrossRef]
22. Tseng, H.-H.; Wey, M.-Y.; Lin, C.-L.; Chang, Y.-C. Pore Structure Effects on Ca-Based Sorbent Sulfation Capacity at Medium Temperatures: Activated Carbon as Sorbent/Catalyst Support. *J. Air Waste Manag. Ass.* **2002**, *52*, 1281–1287. [CrossRef]
23. Yamamoto, M.; Komaki, S.; Nakajima, D.; Matsushima, N.; Liu, D.; Nishioka, M.; Sadakata, M. Enhancement of $Ca(OH)_2$/Fly Ash Sorbent for the Dry-Desulfurization Process. *Energy Fuels* **2006**, *20*, 1901–1905. [CrossRef]
24. Lee, K.T.; Mohamed, A.R.; Bhatia, S.; Chu, K.H. Removal of sulfur dioxide by fly ash/CaO/$CaSO_4$ sorbents. *Chem. Eng. J.* **2005**, *114*, 171–177. [CrossRef]
25. Renedo, M.J.; Fernández-Ferreras, J. Characterization and Behavior of Modified Calcium-Hydroxide-Based Sorbents in a Dry Desulfurization Process. *Energy Fuels* **2016**, *30*, 6350–6354. [CrossRef]
26. Ishizuka, T.; Tsuchiai, H.; Murayama, T.; Tanaka, T.; Hattori, H. Preparation of Active Absorbent for Dry-Type Flue Gas Desulfurization from Calcium Oxide, Coal Fly Ash, and Gypsum. *Ind. Eng. Chem. Res.* **2000**, *39*, 1390–1396. [CrossRef]
27. Ren, G.; Lan, X.; Guo, Z. Difference of flue gas desulfurization performance and desulfurization mechanism of steel slag obtained under various cooling methods. *J. Environ. Chem. Eng.* **2022**, *10*, 109026. [CrossRef]
28. He, D.; Gong, H.; Chen, Y.; Jiao, Z.; Liu, Y.; Zhang, X.; Qin, C.; Yin, H. Experimental and density functional theory study of the synergistic effect between steam and SO_2 on CO_2 capture of calcium-based sorbents. *Fuel* **2021**, *295*, 120634. [CrossRef]
29. Ryu, H.-J.; Grace, J.R.; Lim, C.J. Simultaneous CO_2/SO_2 Capture Characteristics of Three Limestones in a Fluidized-Bed Reactor. *Energy Fuels* **2006**, *20*, 1621–1628. [CrossRef]
30. Xing, G.; Zhao, S.; Li, X.; Qi, L. Mechanism and experimental study of desulfurizing agent based on Mn/Ce-Ca for sintering flue gas desulfurization (FGD). *J. Environ. Chem. Eng.* **2023**, *11*, 111242. [CrossRef]
31. Jia, Y.; Jiang, J.X.; Wang, C.L.; Sun, P.X.; Dong, Y.; Cui, L. Experimental and mechanism study of Ca-based desulfurizer with composite modification for low concentration SO_2 removal under low-temperature. *Process Saf. Environ. Prot.* **2024**, *190*, 1114–1126. [CrossRef]
32. Liao, X.D.; Liu, Y.L.; Liu, Z.S.; Liu, Q.S.; Cen, W.L.; Fan, R.; Li, L.; Shao, J.; Shi, Y.X. Comparative study of pre- and post-Cu modified calcium-based desulfurizers: Experimental and theoretical insights into adsorption vs. catalysis. *J. Environ. Chem. Eng.* **2024**, *12*, 114762. [CrossRef]
33. Veerasingam, S.; Venkatachalapathy, R. Estimation of carbonate concentration and characterization of marine sediments by Fourier Transform Infrared Spectroscopy. *Infrared Phys. Technol.* **2014**, *66*, 136–140. [CrossRef]
34. Busing, W.R.; Levy, H.A. Neutron Diffraction Study of Calcium Hydroxide. *J. Chem. Phys.* **1957**, *26*, 563–568. [CrossRef]
35. Clark, S.J.; Segall, M.D.; Pickard, C.J.; Hasnip, P.J.; Probert, M.I.J.; Refson, K.; Payne, M.C. First principles methods using CASTEP. *Z. Krist. Cryst. Mater.* **2005**, *220*, 567–570. [CrossRef]
36. Perdew, J.P.; Burke, K.; Ernzerhof, M. Generalized Gradient Approximation Made Simple. *Phys. Rev. Lett.* **1996**, *77*, 3865–3868. [CrossRef] [PubMed]